Random forest and live single-cell metabolomics reveal metabolic profiles of human macrophages upon polarization

Tang, H.; Ali, A.M.A.M.; Abdelazem, E.; Ottenhoff, T.H.M.; Heeren, R.M.A.; Mashaghi Tabari, A.

Received: 9 June 2022 | Revised: 5 April 2023 | Accepted: 29 June 2023

DOI: 10.1002/bit.28494

ARTICLE

BIOTECHNOLOGY AND BIOENGINEERING WILEY

Random forest and live single-cell metabolomics reveal metabolic profiles of human macrophages upon polarization

Huaqi Tang[1] | Ahmed Ali[1] | Eman Abdelazem[1] | Tom H. M. Ottenhoff[2] | Ron M. A. Heeren[3] | Alireza Mashaghi[1]

[1]Medical Systems Biophysics and Bioengineering, Leiden Academic Centre for Drug Research, Faculty of Science, Leiden University, Leiden, The Netherlands

[2]Department of Infectious Diseases, Leiden University Medical Center, Leiden, The Netherlands

[3]Division of Imaging Mass Spectrometry, Maastricht MultiModal Molecular Imaging Institute (M4I), Maastricht University, Maastricht, The Netherlands

Correspondence
Ahmed Ali and Alireza Mashaghi, Medical Systems Biophysics and Bioengineering Group, Leiden Academic Centre for Drug Research, Einsteinweg 55, 2333 CC Leiden, The Netherlands.
Email: ali@lacdr.leidenuniv.nl and a.mashaghi.tabari@lacdr.leidenuniv.nl

Funding information
Netherlands Organization for Scientific Research, Grant/Award Numbers: 16249, OCENW. XS2.042; China Scholarship Council

Abstract

Human macrophages are innate immune cells with diverse, functionally distinct phenotypes, namely, pro-inflammatory M1 and anti-inflammatory M2 macrophages. Both are involved in multiple physiological and pathological processes, including would healing, infection, and cancer. However, the metabolic differences between these phenotypes are largely unexplored at single-cell resolution. To address this knowledge gap, an untargeted live single-cell mass spectrometry-based metabolomic profiling coupled with a machine-learning data analysis approach was developed to investigate the metabolic profile of each phenotype at the single-cell level. Results show that M1 and M2 macrophages have distinct metabolic profiles, with differential levels of fatty acyls, glycerophospholipids, and sterol lipids, which are important components of plasma membrane and involved in multiple biological processes. Furthermore, we could discern several putatively annotated molecules that contribute to inflammatory response of macrophages. The combination of random forest and live single-cell metabolomics provided an in-depth profile of the metabolome of primary human M1 and M2 macrophages at the single-cell level for the first time, which will pave the way for future studies targeting the differentiation of other immune cells.

KEYWORDS
human macrophages, phenotype classification, random forest, single-cell metabolomics

1 | INTRODUCTION

Macrophages are critical immune cells known to be highly heterogenous with two major functionally distinct subtypes (Franken et al., 2016; Verreck et al., 2006; Verreck Frank et al., 2004). Namely, classically activated M1 (pro-inflammatory phenotype) and alternatively activated M2 macrophages (anti-inflammatory phenotype), which represent the extreme polarization states of macrophages in response to different environmental changes and stimuli (Yao et al., 2019). M1 macrophages have an enhanced bactericidal and tumoricidal capacity fueled by the production of high levels of pro-inflammatory cytokines. On the other hand, M2 macrophages are commonly associated with the secretion of anti-inflammatory cytokines to promote the resolution of inflammation and facilitate tissue repair and remodeling (Cammarota et al., 2020; Shapouri-Moghaddam et al., 2018;

Verreck et al., 2004, 2006; Zhang et al., 2017). The balance between these two macrophage phenotypes plays a central role in maintaining tissue homeostasis under steady-state conditions and after exposure to pathogens and tissue damage (Abuawad et al., 2020). It is well known that the progression of various inflammatory diseases is also determined by the balance of proper polarization and functioning of the two phenotypes (McWhorter et al., 2013; Raggi et al., 2017). However, the molecular events that control M1 and M2 polarization and the metabolic differences between human M1 and M2 macrophages that determine their distinct functional properties are not fully understood, especially at the single-cell level. There are several limiting factors, among them are the technical limitations associated with analyzing the small volumes of single cells, and the difficulty in extracting meaningful insights from the complex, multidimensional data sets generated from untargeted metabolomics experiments (Evers et al., 2019).

The usage of primary human M1 and M2 macrophages in metabolome comparison studies is currently limited. Previous studies were conducted on murine bone marrow-derived macrophages or immortalized macrophage cell lines (Diskin & Pålsson-McDermott, 2018), all of which have various extents of differences with human primary macrophages. These differences include but are not limited to cell surface markers expression, compound production (e.g., nitric oxide), arginine metabolism, transcriptomic and proteomic profiles, and so on (Andreu et al., 2017; Fuchs et al., 2019; Martinez et al., 2013; Murray & Wynn, 2011; Tedesco et al., 2018; Thomas & Mattila, 2014; Vrieling et al., 2020). Therefore, additional research is needed for better understanding of the correlation between the metabolic state and the phenotypic heterogeneity of macrophages, with particular emphasis on human primary macrophages. Metabolomics is a powerful tool that can achieve this objective by identifying changes in small molecule metabolite profiles and metabolic pathways. However, traditional population-level metabolomic approaches do not consider the inherent cellular heterogeneity and instead average out the metabolic profile across a large number of cells (Evers et al., 2021). This is especially relevant to macrophages, which are known to be heterogenous. Therefore, ignoring cellular heterogeneity may adversely affect biological insights gained from averaged population metabolic studies.

Single-cell metabolomics provide the capability to reveal the cellular metabolic heterogeneity of individual cells that is often masked in pooled analyses (DeVilbiss et al., 2021; Duncan et al., 2019; Kumar et al., 2020). Cellular heterogeneity is ubiquitous but still poorly understood. This is mainly due to the insufficient sensitivity and inapplicability of current technologies to low analyte abundances and limited sample volumes associated with single cells (Ali, Abouleila, Shimizu, Hiyama, Emara, et al., 2019; Yin et al., 2019). Live single-cell mass spectrometry (LSC-MS) is a promising technique that has the required sensitivity and selectivity for single-cell metabolic profiling (Ali, Abouleila, Shimizu, Hiyama, Watanabe, et al., 2019; Duncan et al., 2019; Evers et al., 2021; Okubo-Kurihara et al., 2022). In LSC-MS, a live single cell or single organelle is sampled into a tapered glass microcapillary under microscopic observation with minimal disruption to the cellular microenvironment (Figure 1a). The sampling capillary is then attached to a modified mass spectrometry source where the cellular contents are sprayed, and subsequently measured by mass spectrometry with minimal dilution (Abouleila et al., 2019). This technique has been successfully employed to discern metabolic differences and targeted metabolites analysis for single plant cells, and mammalian cells (Abouleila et al., 2019; Fujii et al., 2015), but never been performed on primary human cells and immune cells. Another reason that hinders the adoption of single-cell metabolic studies is the difficulty of analyzing the complex spectral data sets generated from such experiments. This complexity is largely due to the lack of proper sampling processing and separation, two essential steps in traditional metabolomics experiments that are extremely difficult to implement in single-cell studies due to the low volumes of single cells.

Random forest (RF) is a machine-learning (ML) approach that uses an ensemble classification trees for classification and feature

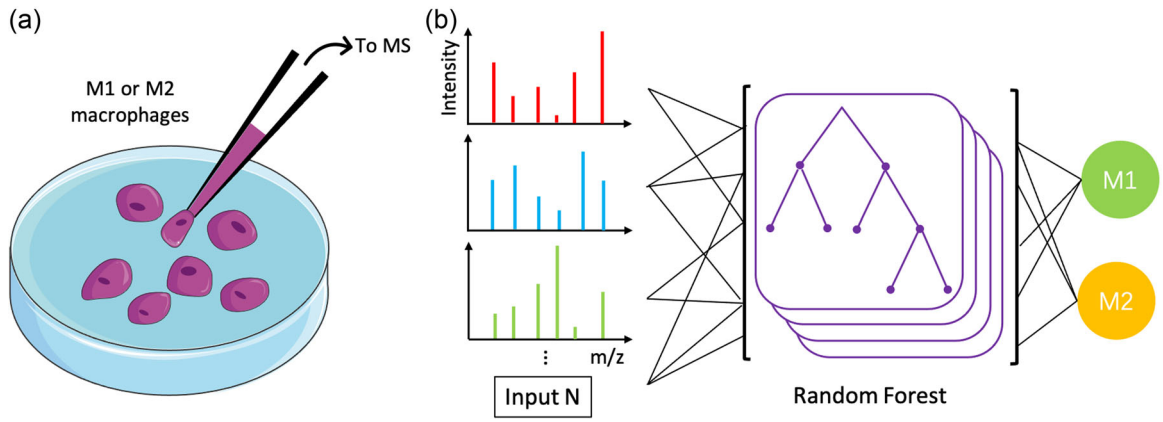

FIGURE 1 Schematic of live single-cell mass spectrometry combined with random forest. (a) Single M1 or M2 macrophage samples were picked up using a tapered glass capillary attached to a micromanipulator, followed by mass spectrometry measurement after adding ionization solvent from the opposite end of the capillary. (b) Random forest model was constructed on the obtained mass spectrometry data sets after data preprocessing to characterize the potential distinct metabolic signature between human M1 and M2 macrophages.

selection (Zhao et al., 2019). RF has been applied in the analysis of population-level metabolome data obtained from mass spectrometry measurements (Liebal et al., 2020), with its unique advantages, namely, high-classification performance, no need of kernel and complex parametrization adjustments, fast at prediction time, and can provide feature importance assessment for the results (Melo et al., 2018). Therefore, it represents a promising candidate as a high-performance classifier based on the mass spectral input data (mass-to-charge ratio [m/z value] × intensity) generated from the analysis of single-cell samples (Figure 1b). Furthermore, features used in the classification can be extracted from the RF model, and then used to identify the peaks unique to each phenotype.

Here, we demonstrate for the first time the applicability of LSC-MS to metabolic analysis of primary human cells, specifically immune cells. To achieve this, an innovative single-cell methodology based on untargeted LSC-MS metabolomic profiling combined with RF was developed and applied to provide an accurate prediction model for metabolomics, and enable single-cell-based discrimination of primary human M1 and M2 macrophages. This platform succeeded in capturing the metabolic signature unique to M1 and M2 macrophages, and then leveraging it to classify each phenotype with a high degree of selectivity and sensitivity, all at the single-cell level. Furthermore, putatively annotated metabolites that are differentially present in each phenotype were extracted from the RF model, such as fatty acyls, glycerophospholipids, and sterol lipids, which are important components of plasma membrane and involved in multiple biological processes such as inflammation and cell differentiation. These findings showcase the potential of using single-cell metabolomics, coupled with RF models to do phenotypical classification based on single-cell metabolomics data, and subsequently, gain a deeper understanding of the metabolome of heterogenous cell populations. This will help fuel the future research that aims to explore modulatory mechanisms of immune cell differentiation at the single-cell level.

2 | MATERIALS AND METHODS

2.1 | Macrophage differentiation

Peripheral blood mononuclear cells were isolated from buffy coats of healthy blood bank donors. Monocytes were isolated through density gradient centrifugation over Ficoll-Paque followed by magnetic-activated cell sorting using CD14 microbeads and differentiated for 6 days into M1 or M2 macrophages with 5 ng/mL of granulocyte-macrophage colony-stimulating factor (GM-CSF; 130-093-864, Miltenyi Biotec) or 50 ng/mL macrophage colony-stimulating factor (M-CSF; 130-096-489, Miltenyi Biotec) respectively. Cells were cultured at 37°C/5% CO_2 in RPMI 1640 medium (31870025, Gibco) supplemented with 10% FBS, 2 mM L-alanyl-L-glutamine (GlutaMAX; 35050038, Gibco), and penicillin-streptomycin (35050038, Gibco). As quality control, macrophages were stained for surface expression of CD14, CD163, and CD11b acquired on a flow cytometry (BD LSRFortessa, BD Biosciences). Macrophage differentiation and activation status was determined by quantifying IL-12 and IL-10 secretion by ELISA following stimulation of cells in the presence of 100 ng/mL lipopolysaccharide for 24 h.

2.2 | Single-cell sample preparation

Single-cell sampling was achieved using a sampling setup which includes a 3D micromanipulator (Narishige) connected to a platinum-coated glass capillary (Humanix) and fixed onto a video microscope (Olympus). Macrophages cultured in a 35 mm petri dish were observed under microscopy, a single M1/M2 macrophage of interest was sucked into a glass capillary (CT-2; Humanix) by applying negative pressure on the sampling capillary with constant visual feedback from the microscope ($n = 23$ for single M1 and $n = 33$ for single M2 samples). Similarly, the culture medium was also sampled as control ($n = 7$). To each capillary, 2 µL of the ionization solvent (a mixture of 80% methanol, 10% dimethyl sulfoxide, and 0.1% formic acid) was introduced from the rear end, followed by the introduction of the capillary's content into the mass spectrometer by applying high voltage to the capillary, where the voltage differential between the capillary and the mass spectrometer's inlet causes the capillary contents to be sprayed into the mass spectrometer for measurement.

2.3 | Mass spectrometry measurement

Mass spectrometry measurements were performed on a Q-Exactive orbitrap mass spectrometer (Thermo Fisher Scientific) equipped with an offline nanoelectrospray source (Nanospray Flex; Thermo Fisher Scientific) to introduce the cellular contents into the instrument. Since the sampling capillaries are coated with platinum, they also act as a nanospray emitter once a voltage differential is established between the capillary and the mass spectrometer inlet. To initiate measurements, the glass capillary was fixed onto the offline nanospray source at 2 mm away from the inlet. Spectra acquisition was done in positive mode, with spray voltage set between 1 and 1.5 kV, to maintain a spray current between 0.1 and 0.12 microampere. The inlet capillary temperature was set to 250°C, instrument resolution to 100,000 full-width half maxima, normalized automatic gain control target to 1e6, and maximum injection time to 500 ms. The mass spectra were obtained in successive SIM regions covering the m/z ranges from 100 to 880 m/z. Each SIM window width was set to 50 m/z. The instrument was calibrated according to the manufacturer's standard operating procedures before the start of measurements every day to make sure that the m/z error does not exceed the accepted values (5 ppm).

2.4 | Data processing

Measured data were converted from the vendor's raw proprietary format to text files by an in-house script after centroiding.

The resulting peak lists were aligned using MarkerView (Sciex) with an m/z threshold of 5 ppm. The aligned peaks were then imported in R statistical software, where the rest of data processing and analysis was done. To check the quality of the MS spectra obtained, the total number of peaks, median measured m/z, and the peak intensities were plotted. Based on the aforementioned data, a total of six samples were eliminated based on their extremely low number of peaks of intensities above 1000 absolute intensity value, indicating an unsuccessful MS run. Of the removed samples, two were M1 cells (n = 21 left), and four were M2 cells (n = 29 left). Background subtraction was achieved by removing peaks in the samples appearing in 75% of the measured blanks. Furthermore, contaminants, salt clusters, and exogenous molecules were removed from the data set by calculating the mass defect of all measured peaks and eliminating those with a characteristically high mass defect (McMillan et al., 2016). Peak intensity values were then log2 transformed, and pareto scaled in preparation for the statistical analysis.

2.5 | Statistical analysis

RF was selected as the ML algorithm of choice due to its good performance in phenotypic discrimination and biomarker isolation (Chen et al., 2013), especially in high-dimensional data sets as is the case in this study.

Highly correlated peak pairs with a Pearson correlation coefficient of more than 0.75 were identified, and one of the peaks in each correlating set was removed to prevent deterioration of the statistical mode performance. Feature selection was then done using recursive feature elimination (RFE) with preset subsets. RFE is an efficient approach for feature selection by eliminating specified proportion of variables with the smallest importance upon each iteration, so that determines a minimal subset of variables needed for an effective model with good prediction accuracy (Acharjee et al., 2020; Darst et al., 2018; Degenhardt et al., 2019). The resultant features were then used in the first RF model. M1 and M2 samples were split randomly into a training set (70% of the samples) and a test set (30% of the samples). The training set was then used for cross-validation of discriminative features identification as shown below, while the test set was set aside for assessing the performance of the RF model later.

Cross-validation was done using successive splits of the training data set to test the performance of the generated model. This was done by manual cross-validation, where the data were randomly split into five subsets. In each subset, an RF model was built to classify both phenotypes. The features that were commonly used by all five cross-validation models were selected and designated as the most common discriminative features. The receiver operating characteristic (ROC) curves of previous models were then plotted.

The identified common discriminative features from the previous step were in the first RF model. The model was tuned by selecting the optimum mtry value that corresponds to the lowest out-of-bag (OOB) error rate. The mtry represents the number of variables randomly sampled as candidates at each split, which is important parameter in RF: individual trees would have poor predictions with a low mtry value, and collection of trees would not diverse enough with high value (Capitaine et al., 2020; Couronné et al., 2018; Wenck et al., 2022). Typically, around 2/3 of samples are used as training set while the remaining is used as test set, termed as the OOB samples (Acharjee et al., 2020; Zhao et al., 2019). OOB is used to access the prediction performance of the model, the lower the OOB error rate, the better the classification (Oza et al., 2019). For the number of trees selection, number of trees versus the OOB were plotted (Figures 2a and 3a) and 500 trees were chosen.

The first model was tested against the test set and by using confusion matrix (Figure 2b) and permutation test. For the permutation test, we developed the permuted model by blinding the samples and randomly assigned M1 and M2 phenotypes to them. We used this data as test for the model and for this permuted data we had an AUC of 0.5 and this confirmed that our model is robust against randomly classified samples. The comparison between the five cross-validation model, permutated model, and the final model was visualized using an ROC curve (Figure 2c).

The features used in the aforementioned model were reduced further by removing peaks with mean signal-to-noise (S/N) ratio < 10 as well as peaks that could not be putatively identified by matching to databases (Human Metabolome Database [HMDB] or Lipidmaps). The resulting final set of discriminative features were used to generate the second, and final RF model, which was cross-validated using a new 80/20 split and a confusion matrix.

The final discriminative features were visualized using most important plot, multidimensional scaling (MDS) plot of the final RF model and a heatmap of the scaled transformed intensities of those peaks. Finally, a t-test was performed on the final discriminative features to test the significance of their abundance between the two phenotypes (M1 and M2). The script used in data processing and analysis is available upon request from the authors.

3 | RESULTS

3.1 | Feature selection and identification of discriminative features

Feature selection was undertaken between M1 (n = 21 after removal) and M2 (n = 29 after removal). Out of the initial 17,364 m/z peaks in the data set, 9770 remained after blank subtraction and highly correlated peaks removal. The RFE designated 170 features as the most important features. This was done using five RF model repeats of the RFE control which gave the highest accuracy (Supporting Information: Figure S1). The 170 features from the RFE control were used to select the most common discriminative features. Samples underwent a 70/30 split, and the 70% portion was split five times into training and test subsets where five cross-validation RFs were done. The top 100 features used in each model were combined and

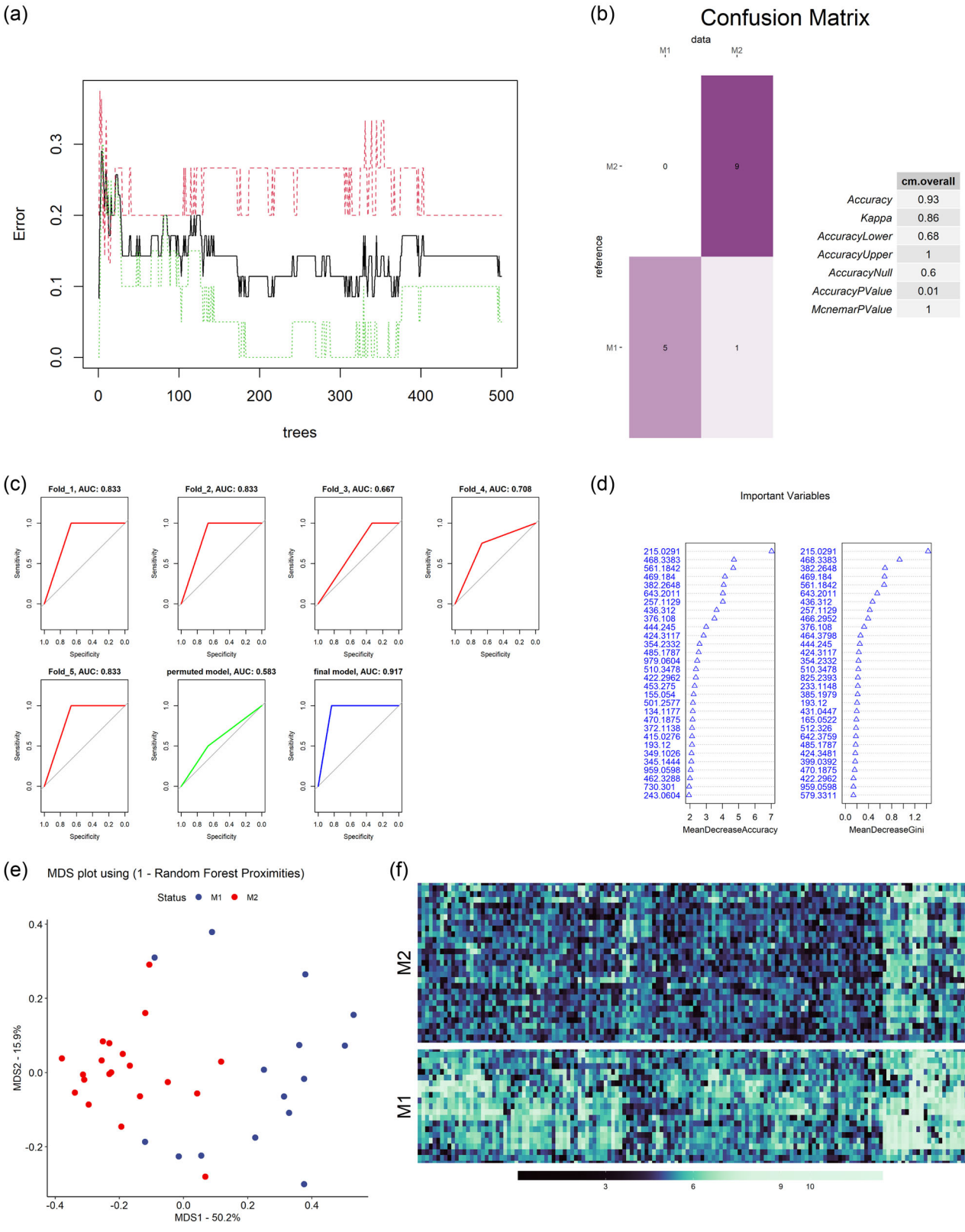

FIGURE 2 (See caption on next page).

designated as the most common discriminative features (151 features, Supporting Information: Table S1).

3.2 | RF model and classification performance

The first RF model was established based on the most common 151 peaks. In total, 500 trees were grown and during the growing, proximities were computed for the cases. Similar cases may fall into the same terminal node or derive from the same parent. After tuning our RF model using 500 trees and mtry = 23 resulted a model had OOB estimate of error rate = 11.43%. The OOB error rate did not decrease with the number of trees constructed, and the RF algorithm could avoid overfitting to a certain extent as shown in Figure 2a. Its classification accuracy was tested using a confusion matrix against the main test data set that was set aside from the beginning and resulted in an accuracy of 0.93 (Figure 2b). The ROC curve coupled with its area under the curve (AUC) was used as a parameter to compare between the RF model, the five cross-validation models and the permutated model (Chen et al., 2013). RF score was used to plot the ROC curve, and to calculate the AUC. The ROC curve shows the correlation between sensitivity and specificity at different cutoffs of the RF score. AUC indicates the performance of the model where a larger value indicates higher prediction ability. The ROC curves and AUC values are shown in Figure 2c with a final value of 0.917 which demonstrates the overall stability of the generated RF model. The mean decrease in accuracy was used to measure the contribution of individual peaks in the RF model, and an alternative approach using mean decrease in Gini index are shown in Figure 2d. To visualize the metabolic profile of the samples, MDS was employed to map them into a lower dimensional space. The MDS plot showed that M1 and M2 cells can be characterized according to their respective features as shown in Figure 2e. To visualize the abundance levels of features in each phenotype, a heatmap was used to map the intensity of the 151 features selected by the RF model in all samples (Figure 2f). These visualized results provide an overview of the metabolic alternations in the two-cell phenotypes, as well as the heterogeneity at the single-cell level.

3.3 | Heterogeneous metabolomic profile and putative metabolites in macrophages

Among the important peaks highlighted by the first RF, a total of 23 potential matches were recognized as putatively heterogeneous metabolites between M1 and M2. This was done by matching their m/z values in Lipidmaps and HMDB databases with 5 ppm tolerance. Using this reduced feature set, an RF model was built and cross-validated using an 80/20 training and test sets. After tuning the model with 500 trees and mtry = 15, The resulting model had an OBB error rate of 12.5% (Figure 3a). The RF classification accuracy was tested using confusion matrix against the test set and resulted in accuracy of 0.9 (Figure 3b). The ROC curves and AUC values are shown in Figure 3c with a final value of 0.87. Important variables plots, MDS plot, and heatmaps were done again with final 23 potential peaks used in the second RF model (Figure 3d–f). T-test was implemented to test the significance of these metabolites by their peak intensity as summarized in Table 1. The classes of metabolites that could be putatively annotated were fatty acyls, sterol lipids, glycerophospholipids, amino acids, and others.

4 | DISCUSSION

In this study, we present a powerful connection of LSC-MS and RF prediction model for metabolomics data analysis. The model was built by combining RF algorithm with RFE and cross-validation to find the features necessary and sufficient to classify single-cell MS data by ranking feature importance. It was then applied to incorporate spectral data from all single-cell samples and isolate the most discriminant feature m/z peaks between polarized macrophages. Furthermore, using this model, we could isolate several putatively annotated molecules that contribute to discriminating macrophages upon different polarization. Although both LSC-MS and RF are well-established and have been largely utilized within their respective fields, the connection of these two provides an alternative to existing approaches given its effective performance on sparse, high-dimensional data with collinear features and straightforward understandability for single-cell data (Park et al., 2020). Despite the

FIGURE 2 Classification performance of the first random forest (RF) model for discriminating M1 and M2 macrophages. (a) Plot of overall out-of-bag (OOB)/overall error rate for RF classification of M1 and M2 versus number of trees. The black curve is the OOB of the model, the green curve is the OOB error rate when classifying M1 (reference), and the red curve is the OOB error rate when classifying M2. (b) Confusion matrix generated after training the first model with the selected peaks. (c) Assessing the performance of RF using cross-validation. A 5-fold cross-validation of the RF model was performed to select the common important peaks by each cross-validated model. The final performance with area under the curve value of 0.917 demonstrates the overall stability of our RF model. (d) The contribution of individual peaks in the RF model. The mean decrease in accuracy and alternative approach using mean decrease in Gini were used to rank the relative importance of individual peaks for metabolic pattern recognition in the RF model. Only the 30 top-ranked peaks and variables for each cell type are shown. (e) Multidimensional scaling plot for mass spectrometry data of M1 and M2. (f) Heatmap of important peaks found in all collected M1 and M2. Heatmap visualizes the intensity of each significant peak measured in all M1 and M2 single-cell samples. The color scales between black and bright green represent lower intensity to higher intensity, respectively.

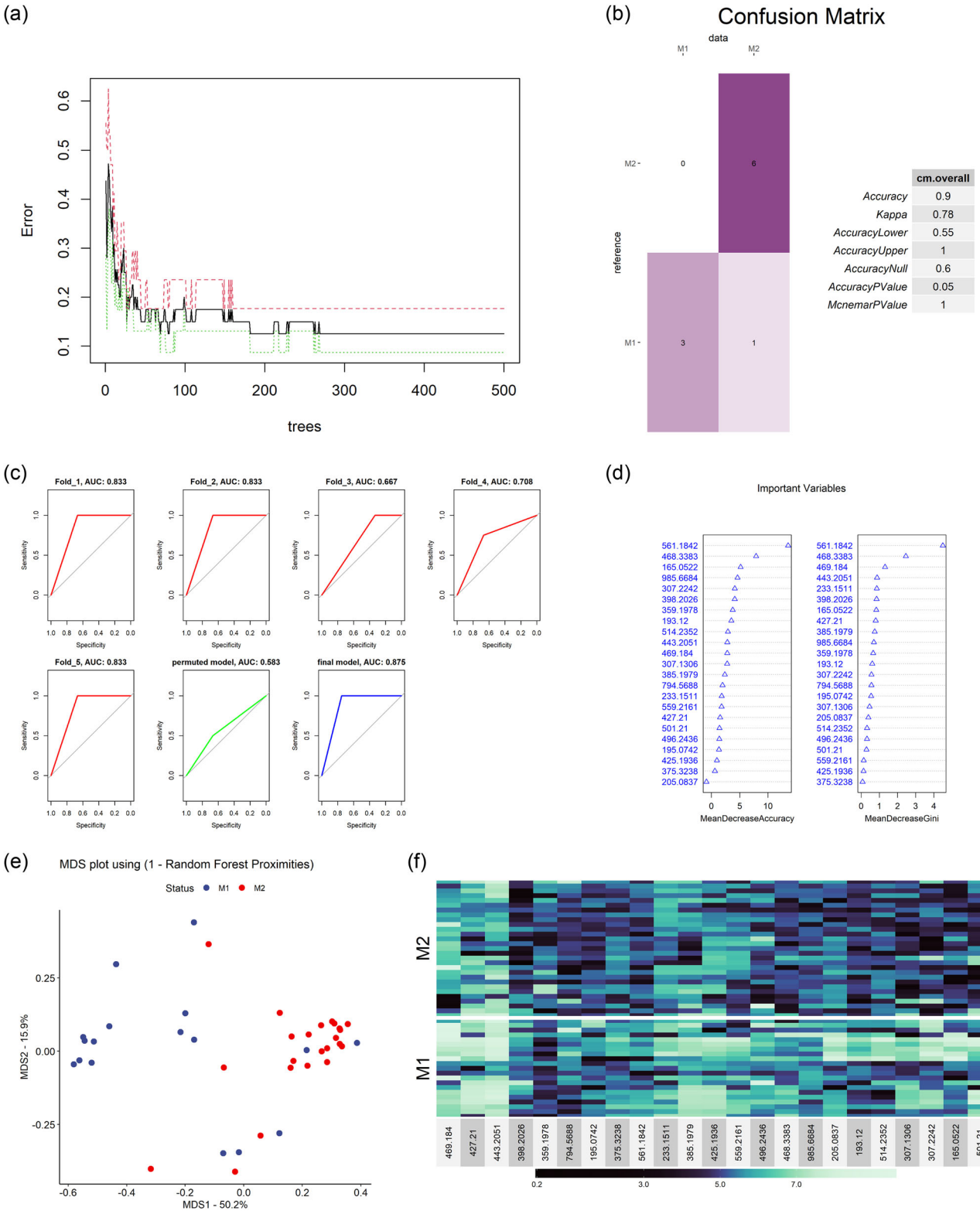

FIGURE 3 Classification performance of the second random forest (RF) model. (a) Plot of overall out-of-bag (OOB) error rate for RF classification of M1 and M2 versus number of trees. The black curve is the OOB (overall error rate) of the model, the green curve is the OOB error rate when classifying M1 (reference), and the red curve is the OOB error rate when classifying M2. (b) Confusion matrix generated after training the second model with the final selected peaks. (c) Assessing the performance of RF using cross-validation with the final performance area under the curve value of 0.875 that demonstrates the overall stability of second RF model. (d) The contribution of individual peaks in the second RF model. The mean decrease in accuracy and mean decrease in Gini were used to rank the relative importance of the 23 selected peaks for each cell type. (e) Multidimensional scaling plot for mass spectrometry data of M1 and M2 using the second RF model. (f) Heatmap of selected 23 peaks found in all collected M1 and M2. The color scales between black and bright green represent lower intensity to higher intensity, respectively.

TABLE 1 Summaries of the discriminatory metabolites between M1 and M2.

m/z	Mean peak intensity in M1	Mean peak intensity in M2	*p* Value	M1 vs. M2	Matches	Class	Database
165.0522	1193.11	81.10	0.0003	M1	FA 7:2;O	Fatty acyls	Lipidmaps
193.12	494.29	90.20	0.0005	M1	FA 10:1 (8-Methylnonenoate)	Fatty acyls	HMDB
195.0742	308.56	105.31	0.0994	M1	Glycylproline Prolylglycine	Amino acids	HMDB
205.0837	1080.60	218.71	0.0083	M1	FA 10:3;O (-)-5-oxo-1,2-campholide	Fatty acyls Prenol lipids	Lipidmaps
233.1511	854.25	429.15	0.2240	M1	WE 13:2 FA 13:2	Fatty acyls	Lipidmaps
307.1306	683.93	120.21	0.0004	M1	Estrone-2,3-quinone Estrone-3,4-quinone ST 18:5;O3	Sterol lipids	Lipidmaps
307.2242	1371.95	212.69	0.00002	M1	FA 17:1;O	Fatty acyls	Lipidmaps
359.1978	33.19	321.53	0.0278	M2	FA 20:4;O (20-HETE)	Fatty acyls	Lipidmaps
375.3238	450.68	243.27	0.0504	M1	WE 23:1 FA 23:1	Fatty acyls	Lipidmaps
385.1979	1297.44	459.10	0.00001	M1	ST 21:3;O5 (Cortisol) 1 alpha, 17 alpha, 21-trihydroxy-20-oxo-22,23,24,25,26,27-hexanorvitamin D3 FA 18:1;O4	Sterol lipids Sterol lipids Fatty acyls	HMDB/Lipidmaps Lipidmaps Lipidmaps
398.2026	325.01	102.01	0.0001	M1	Kinetensin 1-3	Amino acids	HMDB
425.1936	1267.95	476.45	0.0584	M1	ST 23:5;O6 FA 20:3;O5	Sterol lipids Fatty acyls	Lipidmaps
427.21	1908.71	755.79	0.0141	M1	ST 23:4;O6 5,6-Dihydroxyprostaglandin F1a	Sterol lipids Fatty acyls	HMDB
443.2051	3144.80	1206.73	0.0002	M1	PG 12:0	Glycerophospholipids	Lipidmaps
468.3383	538.93	92.90	0.0001	M1	ST 29:1;O2	Prenol lipids	HMDB
469.184	3707.47	1286.36	0.0021	M1	ST 18:4;O2; GlcA	Sterol lipids	Lipidmaps
496.2436	707.71	657.89	0.0033	M1	LPE 18:4	Glycerophospholipids	Lipidmaps
501.21	1570.89	272.76	0.0008	M1	4-Hydroxyandrostenedione glucuronide ST 19:3;O3; GlcA (2-Methoxy-estradiol-17beta 3-glucuronide)	Sterol lipids	HMDB Lipidmaps
514.2352	736.19	45.64	0.0858	M1	LPE 18:3	Glycerophospholipids	Lipidmaps
559.2161	768.97	254.21	0.0159	M1	ST 21:4;O5; GlcA 25-Hydroxyvitamin D3-bromoacetate	Sterol lipids	Lipidmaps
561.1842	318.57	63.22	0.0062	M1	12R-acetoxy-punaglandin 3 12R-acetoxy-7Z-punaglandin 3	Fatty acyls	Lipidmaps
794.5688	481.50	224.41	0.0552	M1	PE 40:5 PC 37:5	Glycerophospholipids Glycerophospholipids	HMDB Lipidmaps
985.6684	373.90	126.04	0.0014	M1	PI 43:1 TG 60:14	Glycerophospholipids Glycerolipids	Lipidmaps

limitations in sample size and the inherent issues associated with single-cell metabolomics; the study successfully demonstrates the applicability of untargeted LSC-MS metabolomic profiling combined with RF for macrophage analysis.

Most of the putatively annotated metabolites belong to lipids. It has been reported previously that lipids, such as fatty acyls, glycerophospholipids, sterol lipids, and so on, are components of the cells' plasma membrane and are involved in multiple biological

processes such as inflammation and cell differentiation (Glass & Olefsky, 2012; Masoodi et al., 2015; Zhang et al., 2017). Their metabolism has a role in the pro- or anti-inflammatory functions of macrophages by meeting energetic requirements and modulating membrane fluidity (Mukundan et al., 2009; Zhang et al., 2017). Our results show an elevated fatty acyls level in M1 compared to M2, this is likely due to the ability of M1 cells to sustain inflammatory responses by biosynthesizing of fatty acids and using them as precursors for the synthesis of inflammatory mediators, while M2 relies on fatty acid oxidation to mediate the resolution of inflammation and tissue repair (Batista-Gonzalez et al., 2020). As the main components of cell membrane, the elevated level of the glycerophospholipids in M1 macrophages are clearly from the increased level of PE 40:5/PC 37:5, PE 42:10, and PI 43:1, which is supported by previous findings that an increase in PC, PE, and PI species in M1 polarization while opposite tendency in M2 (Zhang et al., 2017). Besides, our results show that sterol lipids are another metabolite class pre-eminent in M1, this is in line with previous study that macrophage polarizing to the M1 phenotype has increased cellular cholesterol (Lee et al., 2016), which has been theorized to be a potential mechanism for inflammation (Na et al., 2016). Additionally, we observed M1 has increased level of TG 60:14. This is consistent with the results of previous work on bulk level that M1 has substantially higher levels of TG (Morgan et al., 2021). In particular, TG was recently demonstrated to play important antibacterial roles and its synthesis was demonstrated to be required for macrophage inflammatory functions especially the production of PGE2 (Bosch et al., 2020; Castoldi et al., 2020). Furthermore, cortisol (ST 21:3;O5) was observed, which is a potent mediator of the activity of macrophages and for the regulation of macrophage polarization, via intracrine interaction with glucocorticoid receptors, to finally determine the outcome of infection (Maciuszek et al., 2019, 2020). The only metabolites higher in M2 was FA 20:4;O (20-HETE) which is involved in arachidonic acid metabolism. This is consistent with previous findings which stated that this pathway is the most remarkable lipid metabolism disparity between M1 and M2. This finding reaffirms its pivotal role in determining the phenotype of M2 macrophages and highlights the potential of using it as a biomarker for M2 differentiation (Xu et al., 2021).

Despite its promise, it's worth noting that this method is not without its set of limitations. Single-cell sampling process suffers from low throughput and requires highly skilled operators, applying automated methods or microfluidic techniques may overcome these challenges for large-scale single-cell studies. Although many metabolites were putatively annotated, the limited volume of a single cell makes it difficult to perform exhaustive MS/MS identification. It is important to note that the data obtained from single-cell measurements in the current study is semi-quantitative at best. This is due to the difficulties in incorporating internal standards and homogenizing them with single cell without significant dilution and consequently, loss of signal. Progress in enrichment and separation techniques such as capillary electrophoresis, or miniaturized sample preparation via microfluidics can be utilized to overcome this limitation in a future study. Furthermore, the lack of a separation technique adversely affects the selectivity of the method and makes it difficult to perform structure elucidation, especially in the case of lipids. Thus, further studies involving targeted and quantitative analytical measurements at single-cell level are required to confirm the metabolomic alterations detected.

5 | CONCLUSIONS

This proof-of-concept study presents a powerful combination of high-resolution LSC-MS, an RF prediction model for data analysis and rapid database match to distinguish human M1 and M2 macrophages. This platform is sensitive enough to detect subtle changes in a wide range of metabolites from single-cell macrophage samples upon polarization and successfully characterized the potential distinct metabolic signature of human M1 and M2 macrophages. Given the distinct functions and significant number of diseases involving macrophage immunity, the putative metabolite matches found here may provide better understanding of underlying mechanisms in macrophages polarization. The methodology presented here can be applied to various macrophage biology studies and can be adapted to study other immune and other cells as well.

AUTHOR CONTRIBUTIONS

Alireza Mashaghi conceived and supervised the study. Huaqi Tang and Ahmed Ali conducted the experiments. Huaqi Tang, Ahmed Ali, and Eman Abdelazem analyzed the data. Tom H. M. Ottenhoff provided biological resources and macrophage preparations. Ron M. A. Heeren provided access to the Mass Spectrometry Facility. Huaqi Tang, Ahmed Ali, and Alireza Mashaghi wrote the initial version of the manuscript. All authors revised the manuscript and approved the final version.

ACKNOWLEDGMENTS

This project has been partly funded by the Netherlands Organization for Scientific Research (NWO-TTW, IMMUNMET with grant number 16249, and Open Competition XS with grant number OCENW. XS2.042). Huaqi Tang is financially supported by the CSC Scholarship offered by the China Scholarship Council.

CONFLICT OF INTEREST STATEMENT

The authors declare no conflict of interest.

DATA AVAILABILITY STATEMENT

The data that support the findings of this study are available from the corresponding author upon reasonable request.

ORCID

Alireza Mashaghi http://orcid.org/0000-0002-2157-1211

REFERENCES

Abouleila, Y., Onidani, K., Ali, A., Shoji, H., Kawai, T., Lim, C. T., Kumar, V., Okaya, S., Kato, K., Hiyama, E., Yanagida, T., Masujima, T., Shimizu, Y., & Honda, K. (2019). Live single cell mass spectrometry reveals cancer-specific metabolic profiles of circulating tumor cells. *Cancer Science*, *110*(2), 697–706. https://doi.org/10.1111/cas.13915

Abuawad, A., Mbadugha, C., Ghaemmaghami, A. M., & Kim, D.-H. (2020). Metabolic characterisation of THP-1 macrophage polarisation using LC–MS-based metabolite profiling. *Metabolomics*, *16*(3), 33. https://doi.org/10.1007/s11306-020-01656-4

Acharjee, A., Larkman, J., Xu, Y., Cardoso, V. R., & Gkoutos, G. V. (2020). A random forest based biomarker discovery and power analysis framework for diagnostics research. *BMC Medical Genomics*, *13*(1), 178. https://doi.org/10.1186/s12920-020-00826-6

Ali, A., Abouleila, Y., Shimizu, Y., Hiyama, E., Emara, S., Mashaghi, A., & Hankemeier, T. (2019). Single-cell metabolomics by mass spectrometry: Advances, challenges, and future applications. *TrAC, Trends in Analytical Chemistry*, *120*, 115436. https://doi.org/10.1016/j.trac.2019.02.033

Ali, A., Abouleila, Y., Shimizu, Y., Hiyama, E., Watanabe, T. M., Yanagida, T., & Germond, A. (2019). Single-cell screening of tamoxifen abundance and effect using mass spectrometry and raman-spectroscopy. *Analytical Chemistry*, *91*(4), 2710–2718. https://doi.org/10.1021/acs.analchem.8b04393

Andreu, N., Phelan, J., de Sessions, P. F., Cliff, J. M., Clark, T. G., & Hibberd, M. L. (2017). Primary macrophages and J774 cells respond differently to infection with Mycobacterium tuberculosis. *Scientific Reports*, *7*(1), 42225. https://doi.org/10.1038/srep42225

Batista-Gonzalez, A., Vidal, R., Criollo, A., & Carreño, L. J. (2020). New insights on the role of lipid metabolism in the metabolic reprogramming of macrophages. *Frontiers in Immunology*, *10*, 2993. https://doi.org/10.3389/fimmu.2019.02993

Bosch, M., Sánchez-Álvarez, M., Fajardo, A., Kapetanovic, R., Steiner, B., Dutra, F., Moreira, L., López, J. A., Campo, R., Marí, M., Morales-Paytuví, F., Tort, O., Gubern, A., Templin, R. M., Curson, J. E. B., Martel, N., Català, C., Lozano, F., Tebar, F., … Pol, A. (2020). Mammalian lipid droplets are innate immune hubs integrating cell metabolism and host defense. *Science*, *370*(6514):eaay8085. https://doi.org/10.1126/science.aay8085

Cammarota, E., Soriani, C., Taub, R., Morgan, F., Sakai, J., Veatch, S. L., Bryant, C. E., & Cicuta, P. (2020). Criticality of plasma membrane lipids reflects activation state of macrophage cells. *Journal of the Royal Society Interface*, *17*(163), 20190803. https://doi.org/10.1098/rsif.2019.0803

Capitaine, L., Genuer, R., & Thiébaut, R. (2020). Random forests for high-dimensional longitudinal data. *Statistical Methods in Medical Research*, *30*(1), 166–184. https://doi.org/10.1177/0962280220946080

Castoldi, A., Monteiro, L. B., van Teijlingen Bakker, N., Sanin, D. E., Rana, N., Corrado, M., Cameron, A. M., Hässler, F., Matsushita, M., Caputa, G., Klein Geltink, R. I., Büscher, J., Edwards-Hicks, J., Pearce, E. L., & Pearce, E. J. (2020). Triacylglycerol synthesis enhances macrophage inflammatory function. *Nature Communications*, *11*(1), 4107. https://doi.org/10.1038/s41467-020-17881-3

Chen, T., Cao, Y., Zhang, Y., Liu, J., Bao, Y., Wang, C., Jia, W., & Zhao, A. (2013). Random forest in clinical metabolomics for phenotypic discrimination and biomarker selection. *Evidence-Based Complementary and Alternative Medicine: eCAM*, *2013*, 298183. https://doi.org/10.1155/2013/298183

Couronné, R., Probst, P., & Boulesteix, A.-L. (2018). Random forest versus logistic regression: A large-scale benchmark experiment. *BMC Bioinformatics*, *19*(1), 270. https://doi.org/10.1186/s12859-018-2264-5

Darst, B. F., Malecki, K. C., & Engelman, C. D. (2018). Using recursive feature elimination in random forest to account for correlated variables in high dimensional data. *BMC Genetics*, *19*(1), 65. https://doi.org/10.1186/s12863-018-0633-8

Degenhardt, F., Seifert, S., & Szymczak, S. (2019). Evaluation of variable selection methods for random forests and omics data sets. *Briefings in Bioinformatics*, *20*(2), 492–503. https://doi.org/10.1093/bib/bbx124

DeVilbiss, A. W., Zhao, Z., Martin-Sandoval, M. S., Ubellacker, J. M., Tasdogan, A., Agathocleous, M., Mathews, T. P., & Morrison, S. J. (2021). Metabolomic profiling of rare cell populations isolated by flow cytometry from tissues. *eLife*, *10*, e61980. https://doi.org/10.7554/eLife.61980

Diskin, C., & Pålsson-McDermott, E. M. (2018). Metabolic modulation in macrophage effector function. *Frontiers in Immunology*, *9*, 270. https://doi.org/10.3389/fimmu.2018.00270

Duncan, K. D., Fyrestam, J., & Lanekoff, I. (2019). Advances in mass spectrometry based single-cell metabolomics. *The Analyst*, *144*(3), 782–793. https://doi.org/10.1039/C8AN01581C

Evers, T. M. J., Hochane, M., Tans, S. J., Heeren, R. M. A., Semrau, S., Nemes, P., & Mashaghi, A. (2019). Deciphering metabolic heterogeneity by single-cell analysis. *Analytical Chemistry*, *91*(21), 13314–13323. https://doi.org/10.1021/acs.analchem.9b02410

Evers, T. M. J., Holt, L. J., Alberti, S., & Mashaghi, A. (2021). Reciprocal regulation of cellular mechanics and metabolism. *Nature Metabolism*, *3*(4), 456–468. https://doi.org/10.1038/s42255-021-00384-w

Franken, L., Schiwon, M., & Kurts, C. (2016). Macrophages: sentinels and regulators of the immune system. *Cellular Microbiology*, *18*(4), 475–487. https://doi.org/10.1111/cmi.12580

Fuchs, A. L., Schiller, S. M., Keegan, W. J., Ammons, M. C. B., Eilers, B., Tripet, B., & Copié, V. (2019). Quantitative 1H NMR metabolomics reveal distinct metabolic adaptations in human macrophages following differential activation. *Metabolites*, *9*(11), 248. https://doi.org/10.3390/metabo9110248

Fujii, T., Matsuda, S., Tejedor, M. L., Esaki, T., Sakane, I., Mizuno, H., Tsuyama, N., & Masujima, T. (2015). Direct metabolomics for plant cells by live single-cell mass spectrometry. *Nature Protocols*, *10*(9), 1445–1456. https://doi.org/10.1038/nprot.2015.084

Glass, C. K., & Olefsky, J. M. (2012). Inflammation and lipid signaling in the etiology of insulin resistance. *Cell Metabolism*, *15*(5), 635–645. https://doi.org/10.1016/j.cmet.2012.04.001

Kumar, R., Ghosh, M., Kumar, S., & Prasad, M. (2020). Single cell metabolomics: A future tool to unmask cellular heterogeneity and virus-host interaction in context of emerging viral diseases. *Frontiers in Microbiology*, *11*, 1152. https://doi.org/10.3389/fmicb.2020.01152

Lee, M. K. S., Moore, X.-L., Fu, Y., Al-Sharea, A., Dragoljevic, D., Fernandez-Rojo, M. A., Parton, R., Sviridov, D., Murphy, A. J., & Chin-Dusting, J. P. F. (2016). High-density lipoprotein inhibits human M1 macrophage polarization through redistribution of caveolin-1. *British Journal of Pharmacology*, *173*(4), 741–751. https://doi.org/10.1111/bph.13319

Liebal, U. W., Phan, A. N. T., Sudhakar, M., Raman, K., & Blank, L. M. (2020). Machine learning applications for mass spectrometry-based metabolomics. *Metabolites*, *10*(6), 243. https://doi.org/10.3390/metabo10060243

Maciuszek, M., Klak, K., Rydz, L., Verburg-van Kemenade, B. M. L., & Chadzinska, M. (2020). Cortisol metabolism in carp macrophages: A role for macrophage-derived cortisol in M1/M2 polarization. *International Journal of Molecular Sciences*, *21*(23), 8954. https://doi.org/10.3390/ijms21238954

Maciuszek, M., Rydz, L., Świtakowska, I., Verburg-van Kemenade, B., & Chadzińska, M. (2019). Effects of stress and cortisol on the polarization of carp macrophages. *Fish & Shellfish Immunology*, *94*, 27–37. https://doi.org/10.1016/j.fsi.2019.08.064

Martinez, F. O., Helming, L., Milde, R., Varin, A., Melgert, B. N., Draijer, C., Thomas, B., Fabbri, M., Crawshaw, A., Ho, L. P., Ten Hacken, N. H., Cobos Jiménez, V., Kootstra, N. A., Hamann, J., Greaves, D. R., Locati, M., Mantovani, A., & Gordon, S. (2013). Genetic programs expressed in resting and IL-4 alternatively activated mouse and human macrophages: Similarities and differences. *Blood*, *121*(9), e57–e69. https://doi.org/10.1182/blood-2012-06-436212

Masoodi, M., Kuda, O., Rossmeisl, M., Flachs, P., & Kopecky, J. (2015). Lipid signaling in adipose tissue: Connecting inflammation & metabolism. *Biochimica et Biophysica Acta*, *1851*(4), 503–518. https://doi.org/10.1016/j.bbalip.2014.09.023

McMillan, A., Renaud, J. B., Gloor, G. B., Reid, G., & Sumarah, M. W. (2016). Post-acquisition filtering of salt cluster artefacts for LC-MS based human metabolomic studies. *Journal of Cheminformatics*, *8*(1), 44. https://doi.org/10.1186/s13321-016-0156-0

McWhorter, F. Y., Wang, T., Nguyen, P., Chung, T., & Liu, W. F. (2013). Modulation of macrophage phenotype by cell shape. *Proceedings of the National Academy of Sciences*, *110*(43), 17253–17258. https://doi.org/10.1073/pnas.1308887110

Melo, C. F. O. R., Navarro, L. C., de Oliveira, D. N., Guerreiro, T. M., Lima, E. d. O., Delafiori, J., Dabaja, M. Z., Ribeiro, M. S., de Menezes, M. d. S., Rodrigues, R. G. M., Morishita, K. N., Esteves, C. Z., de Amorim, A. L. L., Aoyagui, C. T., Parise, P. L., Milanez, G. P., do Nascimento, G. M., Ribas Freitas, A. R., Angerami, R., … Catharino, R. R. (2018). A machine learning application based in random forest for integrating mass spectrometry-based metabolomic data: A simple screening method for patients with zika virus. *Frontiers in Bioengineering and Biotechnology*, *6*, 31. https://doi.org/10.3389/fbioe.2018.00031

Morgan, P. K., Huynh, K., Pernes, G., Miotto, P. M., Mellett, N. A., Giles, C., Meikle, P. J., Murphy, A. J., & Lancaster, G. I. (2021). Macrophage polarization state affects lipid composition and the channeling of exogenous fatty acids into endogenous lipid pools. *Journal of Biological Chemistry*, *297*(6), 101341. https://doi.org/10.1016/j.jbc.2021.101341

Mukundan, L., Odegaard, J. I., Morel, C. R., Heredia, J. E., Mwangi, J. W., Ricardo-Gonzalez, R. R., Goh, Y. P. S., Eagle, A. R., Dunn, S. E., Awakuni, J. U. H., Nguyen, K. D., Steinman, L., Michie, S. A., & Chawla, A. (2009). PPAR-δ senses and orchestrates clearance of apoptotic cells to promote tolerance. *Nature Medicine*, *15*(11), 1266–1272. https://doi.org/10.1038/nm.2048

Murray, P. J., & Wynn, T. A. (2011). Protective and pathogenic functions of macrophage subsets. *Nature Reviews Immunology*, *11*(11), 723–737. https://doi.org/10.1038/nri3073

Na, Y. R., Gu, G. J., Jung, D., Kim, Y. W., Na, J., Woo, J. S., Cho, J. Y., Youn, H., & Seok, S. H. (2016). GM-CSF induces inflammatory macrophages by regulating glycolysis and lipid metabolism. *The Journal of Immunology*, *197*(10), 4101–4109. https://doi.org/10.4049/jimmunol.1600745

Okubo-Kurihara, E., Ali, A., Hiramoto, M., Kurihara, Y., Abouleila, Y., Abdelazem, E. M., Kawai, T., Makita, Y., Kawashima, M., Esaki, T., Shimada, H., Mori, T., Hirai, M. Y., Higaki, T., Hasezawa, S., Shimizu, Y., Masujima, T., & Matsui, M. (2022). Tracking metabolites at single-cell resolution reveals metabolic dynamics during plant mitosis. *Plant Physiology*, *189*, 459–464. https://doi.org/10.1093/plphys/kiac093

Oza, V., Aicher, J., & Reed, L. (2019). Random forest analysis of untargeted metabolomics data suggests increased use of omega fatty acid oxidation pathway in *Drosophila Melanogaster* larvae fed a medium chain fatty acid rich high-fat diet. *Metabolites*, *9*(1), 5.

Park, M., Vorperian, S., Wang, S., & Pisco, A. O. (2020). Single-cell identity definition using random forests and recursive feature elimination. *bioRxiv*, *2020*, 233650. https://doi.org/10.1101/2020.08.03.233650

Raggi, F., Pelassa, S., Pierobon, D., Penco, F., Gattorno, M., Novelli, F., Eva, A., Varesio, L., Giovarelli, M., & Bosco, M. C. (2017). Regulation of human macrophage M1–M2 polarization balance by hypoxia and the triggering receptor expressed on myeloid cells-1. *Frontiers in Immunology*, *8*(1097), 1097. https://doi.org/10.3389/fimmu.2017.01097

Shapouri-Moghaddam, A., Mohammadian, S., Vazini, H., Taghadosi, M., Esmaeili, S.-A., Mardani, F., Seifi, B., Mohammadi, A., Afshari, J. T., & Sahebkar, A. (2018). Macrophage plasticity, polarization, and function in health and disease. *Journal of Cellular Physiology*, *233*(9), 6425–6440. https://doi.org/10.1002/jcp.26429

Tedesco, S., De Majo, F., Kim, J., Trenti, A., Trevisi, L., Fadini, G. P., Bolego, C., Zandstra, P. W., Cignarella, A., & Vitiello, L. (2018). Convenience versus biological significance: Are PMA-differentiated THP-1 cells a reliable substitute for blood-derived macrophages when studying in vitro polarization? *Frontiers in Pharmacology*, *9*, 71. https://doi.org/10.3389/fphar.2018.00071

Thomas, A. C., & Mattila, J. T. (2014). "Of mice and men": Arginine metabolism in macrophages. *Frontiers in Immunology*, *5*, 479. https://doi.org/10.3389/fimmu.2014.00479

Verreck, F. A. W., de Boer, T., Langenberg, D. M. L., Hoeve, M. A., Kramer, M., Vaisberg, E., Kastelein, R., Kolk, A., de Waal-Malefyt, R., & Ottenhoff, T. H. M. (2004). Human IL-23-producing type 1 macrophages promote but IL-10-producing type 2 macrophages subvert immunity to (myco)bacteria. *Proceedings of the National Academy of Sciences*, *101*(13), 4560–4565. https://doi.org/10.1073/pnas.0400983101

Verreck, F. A. W., de Boer, T., Langenberg, D. M. L., van der Zanden, L., & Ottenhoff, T. H. M. (2006). Phenotypic and functional profiling of human proinflammatory type-1 and anti-inflammatory type-2 macrophages in response to microbial antigens and IFN-γ- and CD40L-mediated costimulation. *Journal of Leukocyte Biology*, *79*(2), 285–293. https://doi.org/10.1189/jlb.0105015

Vrieling, F., Kostidis, S., Spaink, H. P., Haks, M. C., Mayboroda, O. A., Ottenhoff, T. H. M., & Joosten, S. A. (2020). Analyzing the impact of mycobacterium tuberculosis infection on primary human macrophages by combined exploratory and targeted metabolomics. *Scientific Reports*, *10*(1), 7085. https://doi.org/10.1038/s41598-020-62911-1

Wenck, S., Creydt, M., Hansen, J., Gärber, F., Fischer, M., & Seifert, S. (2022). Opening the random forest black box of the metabolome by the application of surrogate minimal depth. *Metabolites*, *12*(1), 5.

Xu, M., Wang, X., Li, Y., Geng, X., Jia, X., Zhang, L., & Yang, H. (2021). Arachidonic acid metabolism controls macrophage alternative activation through regulating oxidative phosphorylation in PPARγ dependent manner. *Frontiers in Immunology*, *12*, 618501. https://doi.org/10.3389/fimmu.2021.618501

Yao, Y., Xu, X.-H., & Jin, L. (2019). Macrophage polarization in physiological and pathological pregnancy. *Frontiers in Immunology*, *10*, 792. https://doi.org/10.3389/fimmu.2019.00792

Yin, L., Zhang, Z., Liu, Y., Gao, Y., & Gu, J. (2019). Recent advances in single-cell analysis by mass spectrometry. *The Analyst*, *144*(3), 824–845. https://doi.org/10.1039/C8AN01190G

Zhang, C., Wang, Y., Wang, F., Wang, Z., Lu, Y., Xu, Y., Wang, K., Shen, H., Yang, P., Li, S., Qin, X., & Yu, H. (2017). Quantitative profiling of glycerophospholipids during mouse and human macrophage differentiation using targeted mass spectrometry. *Scientific Reports*, *7*(1), 412. https://doi.org/10.1038/s41598-017-00341-2

Zhao, L.-L., Qiu, X.-J., Wang, W.-B., Li, R.-M., & Wang, D.-S. (2019). NMR metabolomics and random forests models to identify potential plasma biomarkers of blood stasis syndrome with coronary heart

disease patients. *Frontiers in Physiology*, *10*, 1109. https://doi.org/10.3389/fphys.2019.01109

SUPPORTING INFORMATION

Additional supporting information can be found online in the Supporting Information section at the end of this article.

How to cite this article: Tang, H., Ali, A., Abdelazem, E., Ottenhoff, T. H. M., Heeren, R. M. A., & Mashaghi, A. (2023). Random forest and live single-cell metabolomics reveal metabolic profiles of human macrophages upon polarization. *Biotechnology and Bioengineering*, *120*, 2314–2325. https://doi.org/10.1002/bit.28494